Scientific Research Publishing

Open Journal of Applied Sciences, 2022, 12, 555-573
https://www.scirp.org/journal/ojapps
ISSN Online: 2165-3925
ISSN Print: 2165-3917

Study on the Influence of Blade Outlet Backsweep Angle on Performance of Impeller

Peng Jiang*, Yong Tian, Bo Wang, Nannan Zhang

Institute of Engineering Thermophysics, Chinese Academy of Sciences, Beijing, China
Email: *jiangpeng8712@163.com

How to cite this paper: Jiang, P., Tian, Y., Wang, B. and Zhang, N.N. (2022) Study on the Influence of Blade Outlet Backsweep Angle on Performance of Impeller. *Open Journal of Applied Sciences*, **12**, 555-573.
https://doi.org/10.4236/ojapps.2022.124039

Received: March 30, 2022
Accepted: April 26, 2022
Published: April 29, 2022

Abstract

As an important parameter of compressor impeller, the design value of blade outlet backsweep angle has a great influence on the performance of impeller. In this paper, six impellers with blade outlet backsweep angle β_{2B} equal to 0˚, 10˚, 20˚, 30˚, 40˚, and 50˚ were designed to evaluate the influences of impeller backsweep angle β_{2B} on the performance, characteristics of gas flow and equivalent stress using computational fluid dynamics (CFD) and finite element analysis (FEA). Results indicated that the performance curve for the outlet backsweep blade angle β_{2B} of 50˚ has the largest stable operating range. The isentropic efficiency of the impeller with backsweep angle β_{2B} equal to 40˚ is 16.8% - 25.9% higher than that of the impeller with backsweep angle β_{2B} equal to 0˚. When the blade outlet backsweep angle is 30˚, the equivalent stress distribution of the impeller is more uniform, the maximum equivalent stress is the smallest.

Keywords

Impeller, Blade Outlet Backsweep Angle, Performance, Isentropic Efficiency, CFD, Secondary Flow

1. Introduction

Centrifugal compressors are often used in thermal machinery, such as turbochargers, turboprop engines, turboshaft engines, and various small jet engines, for laboratory demonstration [1]. A centrifugal compressor has some advantages compared with an axial compressor, such as compact structure, single-stage high pressure ratio, light weight, and so on [2]. Improving efficiency while maintaining mass flow and pressure ratio is the main trend of centrifugal compressor development. As we all know, as the core component of a centrifugal compressor, the performance of the impeller is determined by the radius of the inlet hub, in-

let tip radius, inlet blade angle, outlet radius, outlet width, number of blades, blade outlet angle, tip clearance and so on. Therefore, the structure and aerodynamic design of the impeller are very important to the optimal design of the compressor [3]. Based on the mathematical model or experimental research of gas dynamics, scholars have done a lot of work to explore the influence of the impeller structure of a centrifugal compressor on its efficiency. Maofei *et al.* [4] applied a numerical simulation method to analyze variations in CC performance parameters, polytropic efficiency, and pressure ratio. Senoo [5] found that the tip clearance flow loss is proportional to clearance size. The performance of the compressor was investigated using a numerical approach by Pelz and Karsdadt [6] and Jia *et al.* [7]. Shibata *et al.* [8] designed, manufactured, and tested five types of unshrouded impellers to evaluate the effects of blade loading, backsweep angle, and relative velocity diffusion ratio on the compressor performance. In order to study the influence of varying blade meridional contour on the total pressure ratio and isentropic efficiency from stall to choke, a numerical investigation of the high-pressure ratio turbocharger centrifugal compressor impeller was carried out by Khan *et al.* [9]. Xu *et al.* [10] found that proper meridional profiles can increase the pressure ratio and improve the compressor efficiency at the same blade back curvature. Through numerical simulation, the importance of geometric and design parameters changes with different outlet blade widths and their influence on compressor performance were studied by Rathore and Ravichandrakumar [11]. Xie *et al.* [12] carried out studies to put forwards an optimal design method and investigate the influence of the meridional contour of a steam centrifugal compressor on aerodynamic performance. A turbocharger centrifugal compressor with a vaneless diffuser was studied by Mojaddam and Pullen [13] and the parameters studied included meridional geometry, start location of the main blades and splitters and rotor blade angle distribution. Based on sensitivity analysis and computational fluid dynamics simulation, Ju and Zhang [14] optimized the multi-objective design of series impellers and found that the blade shape of the inducer and the geometry of inducer-inducer clearance had the greatest influence on the efficiency of series impellers. Torshizi *et al.* [15] studied the effect of changing the splitter configuration, and found that the new impeller was subsequently installed on the turbocharger shaft, and the experimental test was carried out under a wide range of operating conditions, which led to an increase of 2.3% in efficiency. The application of the Kriging model in centrifugal impeller optimization was studied by Wang *et al.* [16], and the isentropic efficiency of the design point was increased by 2.49%.

As an important parameter of compressor impeller, the design value of blade outlet backsweep angle has a great influence on the performance of impeller. Studying the influence of the blade outlet backsweep angle of the impeller on the performance of the impeller is helpful to better optimize the design of the impeller. At the same time, there are virtually few studies related to the influence of blade outlet backsweep angle on the performance of impeller. The purpose of this study is to obtain data on the effect of the blade outlet angle of the impeller

on the performance, characteristics of gas flows and equivalent stress using computational fluid dynamics (CFD) and finite element analysis (FEA), and to subject the numerical results to the empirical correlation development to assist the design and optimize the parameters of the blade to improve impeller performance.

The design and numerical model are presented in Section 2. The software ANSYS CFX is used to get the solution. Theoretical analysis is presented in Section 3. Effects of different blade outlet backsweep angle β_{2B} on total pressure ratio, isentropic efficiency, and power are presented in Sections 4 - 6 and the empirical correlations are presented in Section 7. The effects of different blade outlet backsweep angles on characteristics of gas flow and equivalent stress are presented in Sections 8 - 9. Finally, a summary of the present work is presented in Section 10.

2. Design and Numerical Model

The design of the air compressor is depicted in Figure 1, which illustrates the impeller, diffuser and volute.

Diagrams of impeller parameters are depicted in Figure 2. Structural parameters of six kinds of impellers are shown in Table 1. The impeller inlet hub radius

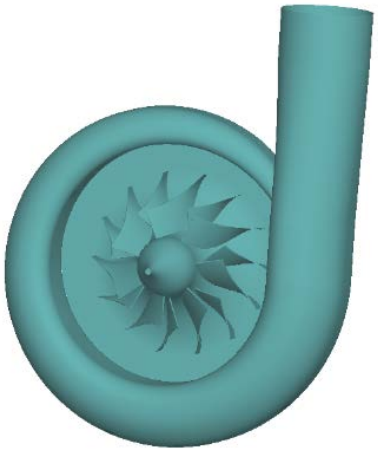

Figure 1. Air compressor.

Table 1. Structural parameters of six kinds of impellers.

NO.	R_{1H}/mm	R_{1T}/mm	β_{1B}/˚	R_2/mm	B_2/mm	β_{2B}/˚
1	39	79	−52	121	23.7	0
2	39	79	−52	121	23.7	10
3	39	79	−52	121	23.7	20
4	39	79	−52	121	23.7	30
5	39	79	−52	121	23.7	40
6	39	79	−52	121	23.7	50

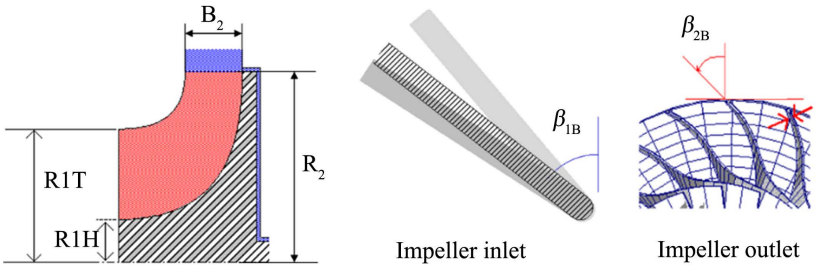

Figure 2. Diagrams of impeller parameters.

R_{1H} was 39 mm, the impeller inlet tip radius R_{1T} was 79 mm, the inlet blade angle β_{1B} of the main blade was −52˚, the impeller outlet radius R_2 was 121 mm, the impeller outlet width b_2 was 23.7 mm, the number of blades (including splitter blades) was 14, and the rated speed n was 26,000 rpm, the tip clearance was 0.3 mm. The blade outlet backsweep angle β_{2B} had values of 0˚, 10˚, 20˚, 30˚, 40˚ and 50˚.

As depicted in **Figure 3**, because of the circular symmetry of the impeller, the single-passage steady-state model was chosen as the numerical calculation model. The H/J/C/L hybrid grid was generated by the grid generation software ANSYS TurboGrid, and then the grid was imported into ANSYS CFX to get the solution. The target passage mesh size of the grid division method was adopted. The maximum expansion rate of the boundary layer was set to 1.2. As shown in **Figure 4**, there are 10 layers of grids in the tip clearance area. The mesh number of the single-passage model was approximately 250,000. As shown in **Figure 5**, the grid independence of the calculation model was verified. The distribution of y_+ was shown in **Figure 6** and the average wall y_+ was around 40. A k-ε turbulence model was chosen to calculate the flow. The working medium was air ideal gas. The inlet total pressure and inlet total temperatures were 101.3 kPa and 20˚C respectively. Tip clearance at shroud was 0.3 mm. The convergence precision of all root-mean-square residuals was less than 10E−5.

A mathematical model is constructed using the following equations [17] based on assumptions:

Continuity Equation:

$$\frac{\partial u}{\partial x}+\frac{\partial v}{\partial y}+\frac{\partial w}{\partial z}=0 \tag{1}$$

where u, v and w are the velocity components and x, y and z are Cartesian coordinates respectively.

Momentum Equation:

In the x-direction,

$$u\frac{\partial u}{\partial x}+v\frac{\partial u}{\partial y}+w\frac{\partial u}{\partial z}=-\frac{1}{\rho_f}\frac{\partial p}{\partial x}+\frac{\mu_f}{\rho_f}\left(\frac{\partial^2 u}{\partial x^2}+\frac{\partial^2 u}{\partial y^2}+\frac{\partial^2 u}{\partial z^2}\right) \tag{2}$$

In the y-direction,

$$u\frac{\partial v}{\partial x}+v\frac{\partial v}{\partial y}+w\frac{\partial v}{\partial z}=-\frac{1}{\rho_f}\frac{\partial p}{\partial y}+\frac{\mu_f}{\rho_f}\left(\frac{\partial^2 v}{\partial x^2}+\frac{\partial^2 v}{\partial y^2}+\frac{\partial^2 v}{\partial z^2}\right) \tag{3}$$

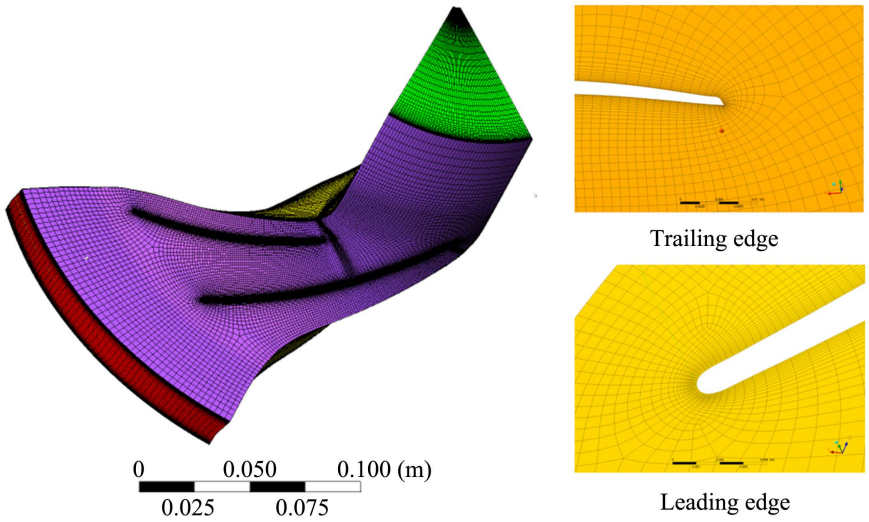

Figure 3. Single-passage steady-state model of the impeller.

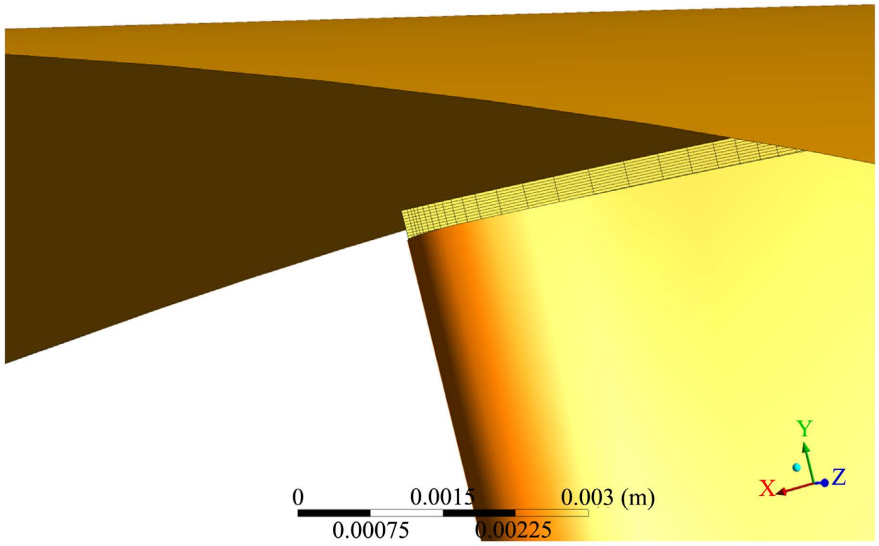

Figure 4. Details of grids in the tip clearance region.

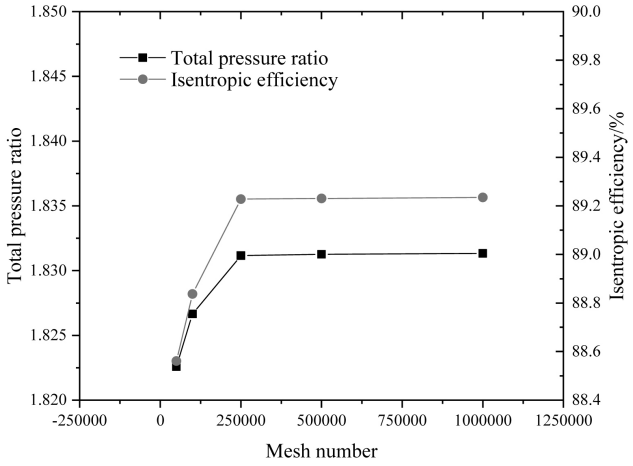

Figure 5. Mesh independency investigation.

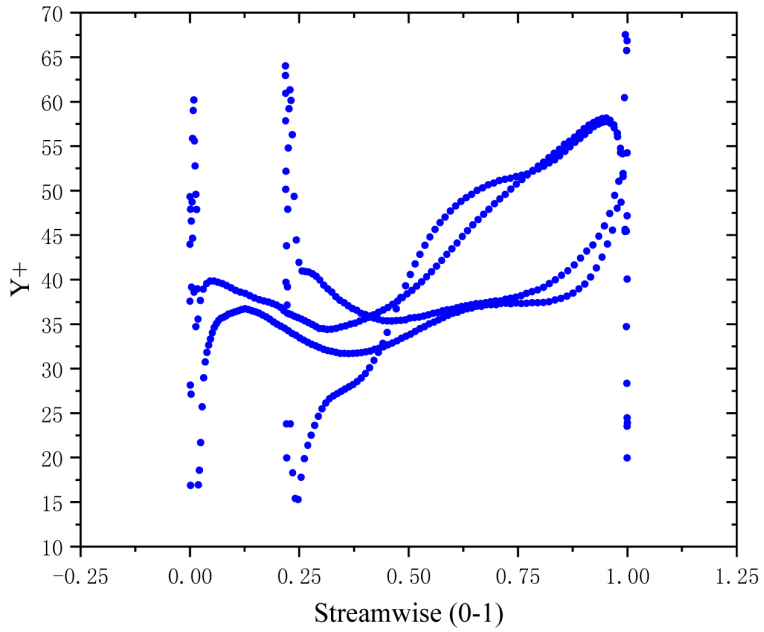

Figure 6. Distribution of y_+.

In the z-direction,

$$u\frac{\partial w}{\partial x}+v\frac{\partial w}{\partial y}+w\frac{\partial w}{\partial z}=-\frac{1}{\rho_f}\frac{\partial p}{\partial z}+\frac{\mu_f}{\rho_f}\left(\frac{\partial^2 w}{\partial x^2}+\frac{\partial^2 w}{\partial y^2}+\frac{\partial^2 w}{\partial z^2}\right) \tag{4}$$

where μ_f and ρ_f are the dynamic viscosity and density of the working fluid, respectively.

Energy Equation:

$$u\frac{\partial T_f}{\partial x}+v\frac{\partial T_f}{\partial y}+w\frac{\partial T_f}{\partial z}=-\frac{k_f}{\rho_f C_{pf}}\frac{\partial p}{\partial z}+\left(\frac{\partial^2 T_f}{\partial x^2}+\frac{\partial^2 T_f}{\partial y^2}+\frac{\partial^2 T_f}{\partial z^2}\right) \tag{5}$$

where T_f, C_{pf} and k_f are the temperature, constant specific heat capacity of the working fluid and thermal conductivity.

3. Theoretical Analysis

As shown in **Figure 7**, the exit velocity triangle is mainly composed of relative velocity W_2, implicated velocity U_2 and absolute velocity C_2. If the slip flow phenomenon is ignored, the tangential velocity component at the outlet of the backward curved impeller can be expressed as Equation (6).

$$C_{\theta 2}=C_{\theta 2\infty}=U_2-C_{m2}\tan\beta_{2B} \tag{6}$$

where $C_{\theta 2}$, U_2, C_{m2} and β_{2B} are the tangential velocity component, circle line speed, meridian velocity and backsweep angle of the blade exit.

Considering the influence of the slip phenomenon, the tangential velocity component at the outlet of the backward curved impeller can be expressed as Equation (7).

$$C_{\theta 2}=U_2-C_{m2}\tan\beta_2 \tag{7}$$

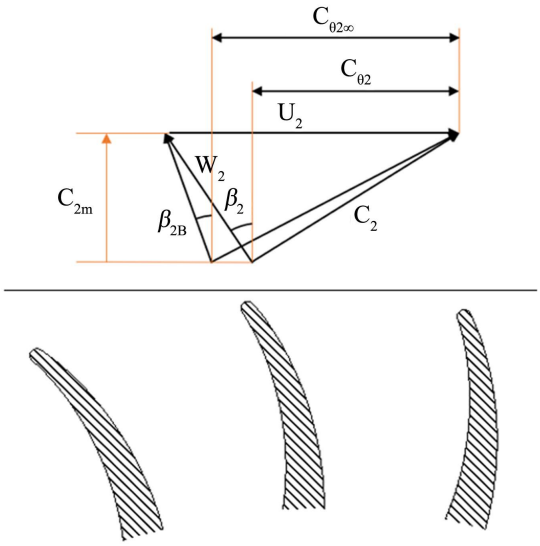

Figure 7. Sketch of exit velocity triangle.

where β_2 is the relative airflow angle of the blade exit. Moreover, in the backward bending impeller, the relative airflow angle β_2 of the blade exit is generally larger than the backsweep angle. Since the tangential velocity component of the blade exit can affect the pressure ratio and power of the impeller, the backward bending angle of the impeller will affect its performance of the impeller.

4. Different Blade Outlet Backsweep Angle β_{2B} Effects on Total Pressure Ratio

As shown in Figure 7, the total pressure ratio is defined as:

$$\Pi_{tot} = \frac{p_{tot,o}}{p_{tot,i}} \tag{8}$$

where $p_{tot,i}$ is the time-averaged total pressure at the entrance section, $p_{tot,o}$ is the time-averaged total pressure at the outlet.

As shown in Figure 8, the total pressure ratio decreases with the increase in mass flow rate. The larger the blade outlet angle is, the smaller the pressure ratio becomes. This is mainly because the tangential component of the outlet velocity decreases with the increase of the outlet backsweep angle at the same flow rate, which reduces the pressure ratio of the impeller. The performance curve for the blade outlet backsweep angle of 50˚ has the largest stable operating range among others. The stable operating range with the blade outlet backsweep angle β_{2B} equal to 50˚ is about 3 times more than that with the blade outlet backsweep angle β_{2B} equal to 0˚. This is mainly because the greater the blade outlet backsweep angle, the more obvious the tangential component of the outlet speed changes with the flow rate, which leads to the more obvious change of the pressure ratio, so that the impeller has a larger stable working range. In order to achieve the same flow rate and pressure ratio as the impeller with a low backsweep angle, it is necessary to increase the impeller speed or increase the impeller outlet radius.

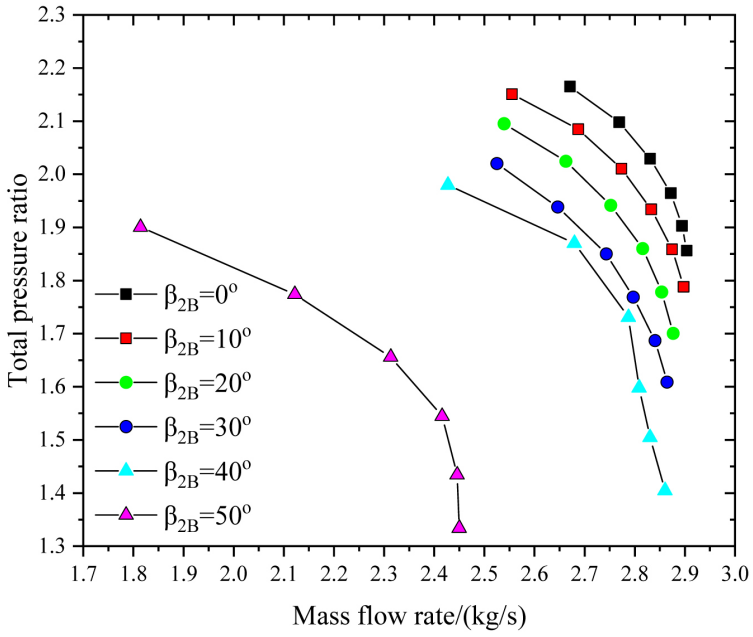

Figure 8. Total pressure ratio versus mass flow rate for different values of blade outlet angle β_{2B}.

5. Different Blade Outlet Backsweep Angle β_{2B} Effects on Isentropic Efficiency

In engineering analysis, the isentropic efficiency is a parameter to measure the degradation degree of energy, which involves the comparison between the machine performances under idealized circumstances and an actual situation for the same inlet and exit states [18]. The isentropic efficiency [19] is defined as Equation (9).

$$\eta = \frac{h_{isen} - h_{in}}{h_{out} - h_{in}} \tag{9}$$

As shown in **Figure 9**, the isentropic efficiency decreases with the increase in mass flow rate. In the range of blade outlet backsweep angle β_{2B} of 0˚ - 40˚, the larger the blade outlet backsweep angle β_{2B} is, the larger isentropic efficiency becomes. In the large mass flow rate region, the curves intersect. This is because a compressor with a large blade outlet angle more easily enters the stall region, where the isentropic efficiency drops rapidly. Both the isentropic efficiency and operating ratio of the impeller with the blade outlet backsweep angle β_{2B} equal to 50˚ are smaller than those with the blade outlet backsweep angle β_{2B} equal to 40˚. The isentropic efficiency of the impeller with backsweep angle β_{2B} equal to 40˚ is 16.8% - 25.9% more than that of the impeller with backsweep angle β_{2B} equal to 0˚.

6. Different Blade Outlet Backsweep Angle β_{2B} Effects on Power

According to energy conservation, the consumed power of compressors is

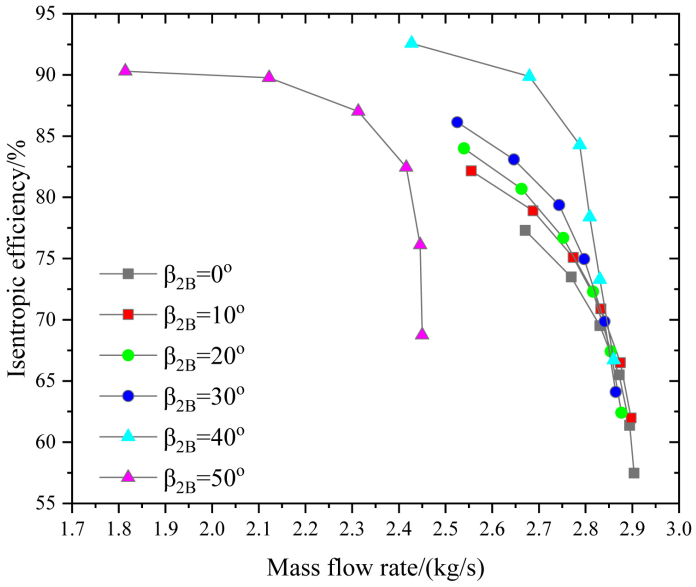

Figure 9. Isentropic efficiency versus mass flow rate for different values of blade outlet angle β_{2B}.

converted into the internal energy of the working medium. This means that the increment of the internal energy of the working medium between the entrance and exit can be used to calculate the indicated power as follows.

$$P = Q_m \left(h_{out} - h_{in} \right) \tag{10}$$

As shown in **Figure 10**, the power decreases with the increase of blade outlet backsweep angle at the same flow rate. This is mainly because the larger the backsweep angle, the smaller the impeller pressure ratio at the same rotation speed and mass flow rate, resulting in the reduction of the required power. When the backsweep angle β_{2B} is equal to 0˚ and 10˚, the power increases monotonously with the increase of mass flow rate. However, the power increases first and then decreases with the increase of mass flow rate when the backsweep angle β_{2B} is equal to 20˚, 30˚, 40˚ and 50˚.

7. Empirical Correlations

The numerical results were subjected to the empirical correlation development to assist the design and optimize the parameters of the blade to improve the impeller performance. The resultant correlations are summarized in **Table 2**, where a_1, a_2, a_3, b_1, b_2, b_3, c_1, c_2 and c_3 are the fitted coefficients.

The comparisons between the fitted data of total pressure ratio correlation, isentropic efficiency correlation and power correlation, and the numerical data are demonstrated in **Figures 11(a)-(c)**. It is calculated by Equation (11). As shown, the fitted data are agreeing with the numerical data within ±15%, ±15% and ±15% except for few points, for total pressure ratio (Π_{tot}), isentropic efficiency (η) and power (P), respectively.

Error = (Predicted data − Numerical data)/Numerical data × 100% (11)

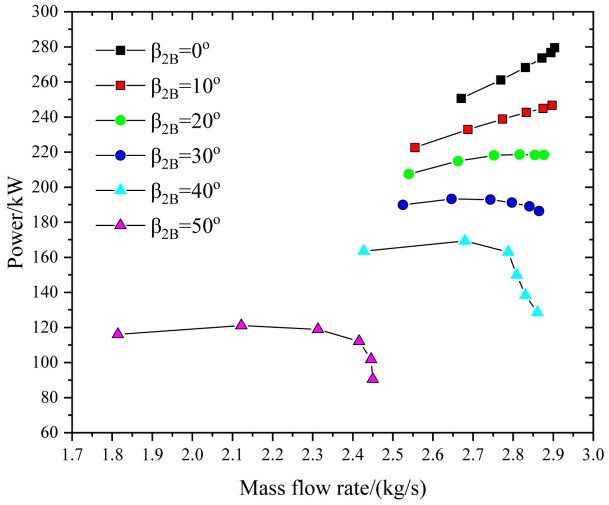

Figure 10. Power versus mass flow rate for different values of blade outlet backsweep angle β_{2B}.

Table 2. Summary of empirical correlations.

Total pressure ratio
$\Pi_{tot} = a_1\left(\frac{\beta_{2B}}{180^\circ}\pi + 1\right)^{a_2} Q_m^{a_3}$, $a_1 = 3.94$, $a_2 = -0.528$, $a_3 = -0.608$
Isentropic efficiency (%)
$\eta = b_1\left(\frac{\beta_{2B}}{180^\circ}\pi + 1\right)^{b_2} Q_m^{b_3}$, $b_1 = 142.15$, $b_2 = 0.132$, $b_3 = -0.697$
Power (kW)
$P = c_1\left(\frac{\beta_{2B}}{180^\circ}\pi + 1\right)^{c_2} Q_m^{c_3}$, $c_1 = 163.7$, $c_2 = -1.185$, $c_3 = 0.549$

8. Different Blade Outlet Backsweep Angle β_{2B} Effects on Characteristics of Gas Flow

The secondary flow is a minor flow, which superimposes the mainflow and causes strong recirculation [8]. In Figures 12-14, the velocity distributions are shown for β_{2B} = 0˚, 10˚, 20˚, 30˚, 40˚, 50˚ for 90% span. In the test case of design centrifugal compressors shown on the blade to blade surface, the velocity at the blade leading edge appears to be higher than that at the blade trailing edge. The secondary flow occurs near the exit tip of the impeller blade. This flow separation causes strong circulatory flow which influences the performance of the impeller. The secondary flow is mainly produced near the outlet pressure surface of the blade when the backsweep angle β_{2B} is equal to 0˚, 10˚, 20˚, 30˚. The secondary flow occurs near the suction surface at the outlet of the blade when the backsweep angle β_{2B} is equal to 40˚, and the effect of the secondary flow increases with the increase of the backsweep angle. When the blade outlet backsweep angle β_{2B} is equal to 40˚, the secondary flow effect is the weakest.

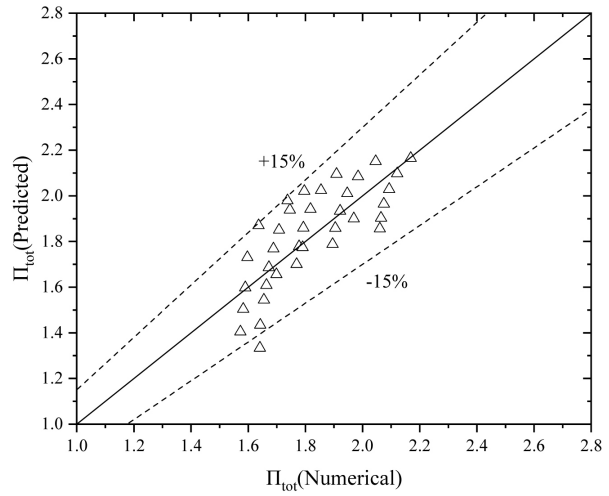

(a)

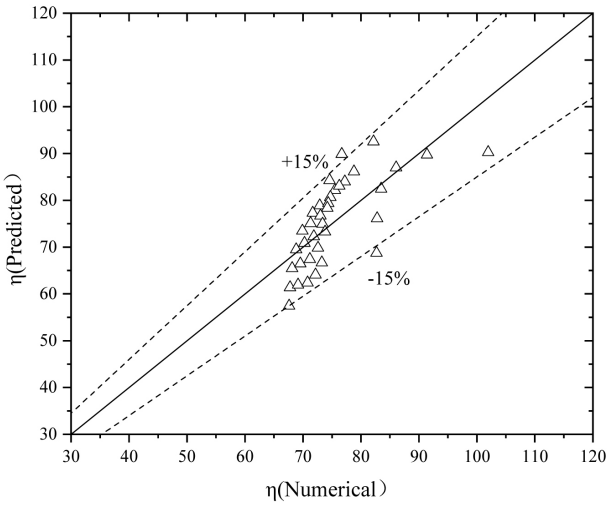

(b)

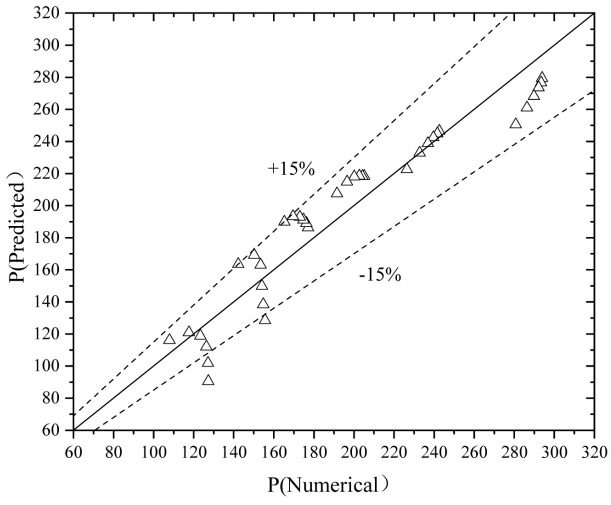

(c)

Figure 11. Comparison between predicted and numerical results (a) total pressure ratio, (b) isentropic.

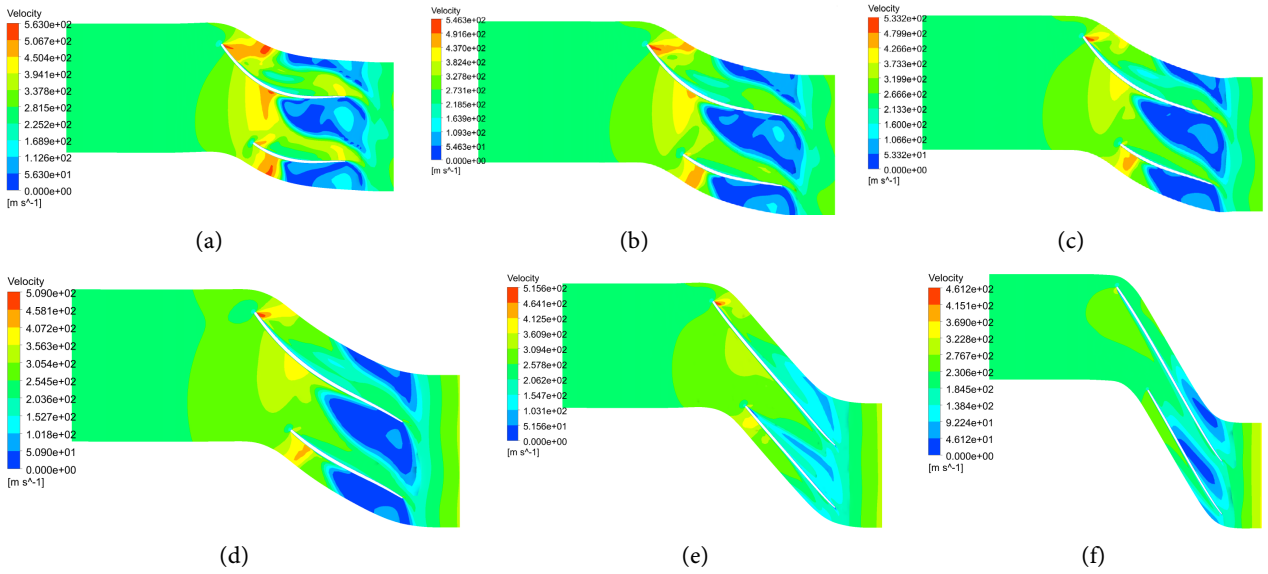

Figure 12. Velocity contour at 90% span at total pressure ratio 1.86. (a) $\beta_{2B} = 0^{\circ}$; (b) $\beta_{2B} = 10^{\circ}$; (c) $\beta_{2B} = 20^{\circ}$; (d) $\beta_{2B} = 30^{\circ}$; (e) $\beta_{2B} = 40^{\circ}$; (f) $\beta_{2B} = 50^{\circ}$.

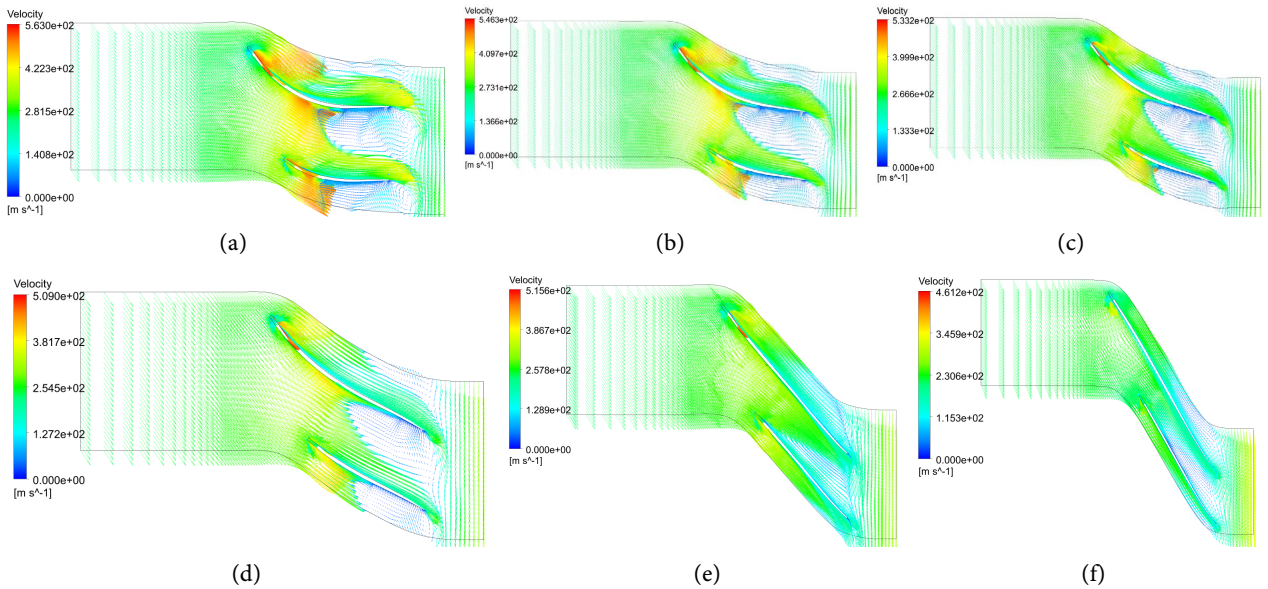

Figure 13. Velocity vector diagram contour at 90% span at total pressure ratio 1.86. (a) $\beta_{2B} = 0^{\circ}$; (b) $\beta_{2B} = 10^{\circ}$; (c) $\beta_{2B} = 20^{\circ}$; (d) $\beta_{2B} = 30^{\circ}$; (e) $\beta_{2B} = 40^{\circ}$; (f) $\beta_{2B} = 50^{\circ}$.

Meridional velocity contour can be efficiently used to study the flow separation in the centrifugal compressor. As it is clear from Figure 15, the flow separation is maximum at the shroud surface because at the shroud surface the meridional velocity is stagnant. If we compare the designs with different blade outlet backsweep angle β_{2B}, then flow separation can be observed lower when the blade outlet backsweep angle β_{2B} is equal to 40˚ and 50˚. This flow separation causes a reduction in isentropic efficiency, pressure ratio, and operating range. This is mainly because the working point of the impeller is closer to the stall zone when the blade outlet backsweep angle β_{2B} is equal to 0˚, 10˚, 20˚and 30˚.

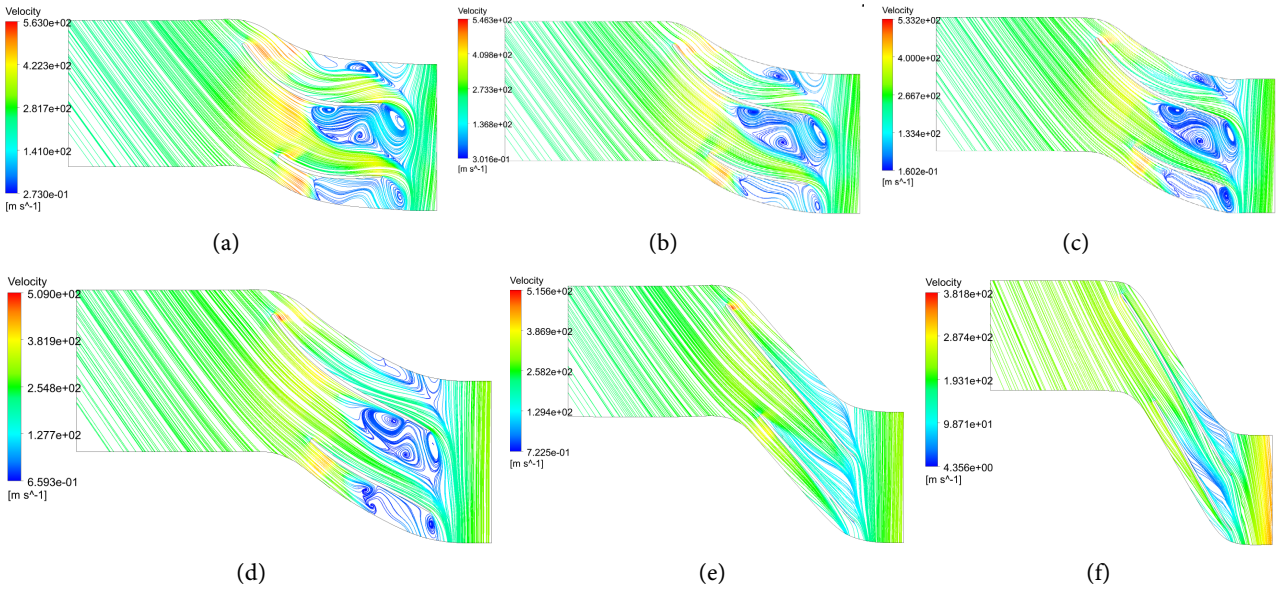

Figure 14. Velocity streamlines at 90% span at total pressure ratio 1.86. (a) $\beta_{2B} = 0^{\circ}$; (b) $\beta_{2B} = 10^{\circ}$; (c) $\beta_{2B} = 20^{\circ}$; (d) $\beta_{2B} = 30^{\circ}$; (e) $\beta_{2B} = 40^{\circ}$; (f) $\beta_{2B} = 50^{\circ}$.

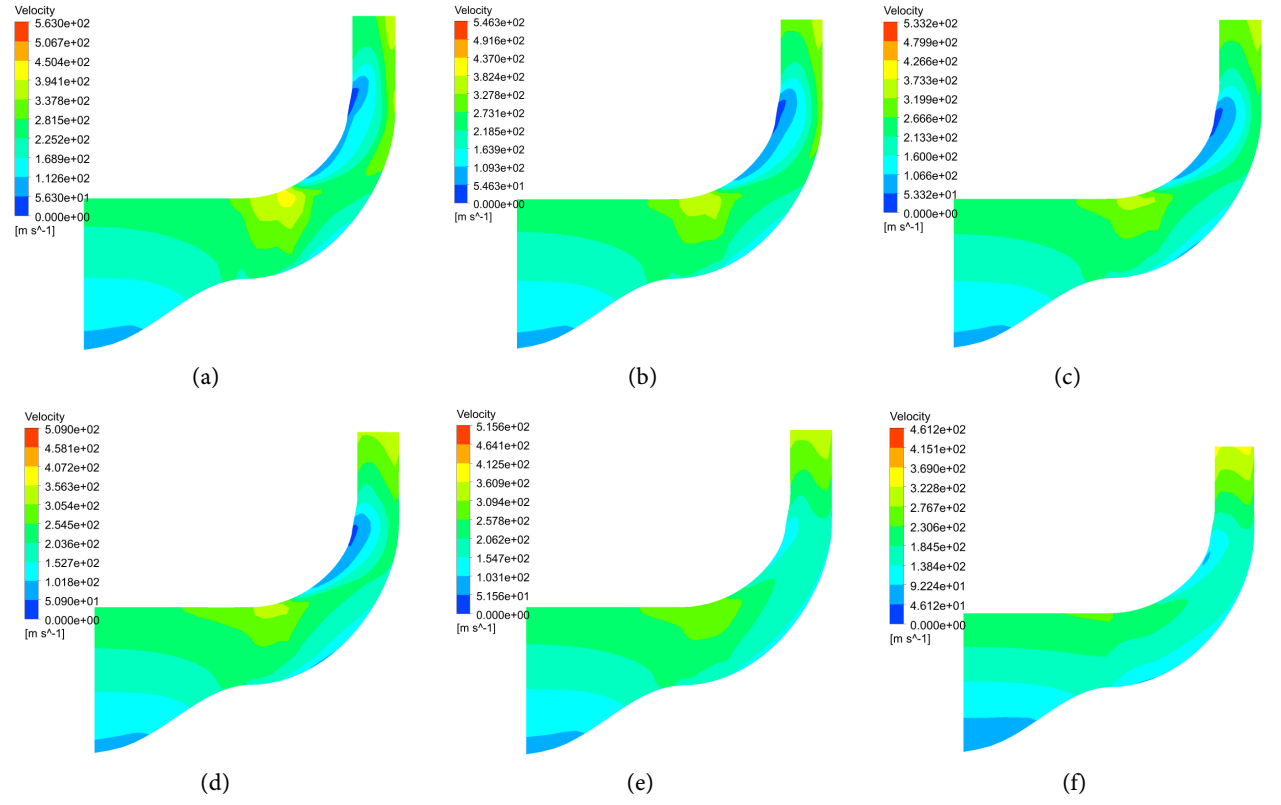

Figure 15. Meridional velocity contours at total pressure ratio 1.86. (a) $\beta_{2B} = 0^{\circ}$; (b) $\beta_{2B} = 10^{\circ}$; (c) $\beta_{2B} = 20^{\circ}$; (d) $\beta_{2B} = 30^{\circ}$; (e) $\beta_{2B} = 40^{\circ}$; (f) $\beta_{2B} = 50^{\circ}$.

9. Different Blade Outlet Backsweep Angle β_{2B} Effects on Equivalent Stress

The material of the impeller was aluminium alloy. The material parameters were

shown in Table 3. As depicted in Figure 16, a mesh generation software ANSYS meshing was used to generate a grid. The mesh number of the single-passage model was approximately 910,000. This was considered sufficiently reliable to ensure mesh independence according to Figure 17. The rotational speed was set to 26,000 rpm.

The equivalent stress of impellers with six different blade outlet backsweep angles β_{2B} was calculated. The maximum equivalent stress is shown in Table 4 and the obtained stress contours are shown in Figure 18. With the increase of the backward bending angle of the blade outlet, the position of the maximum equivalent stress shifts from the inlet tip to the outlet. When the blade outlet backsweep angle is equal to 50˚, the maximum equivalent stress occurs at the root of the blade outlet.

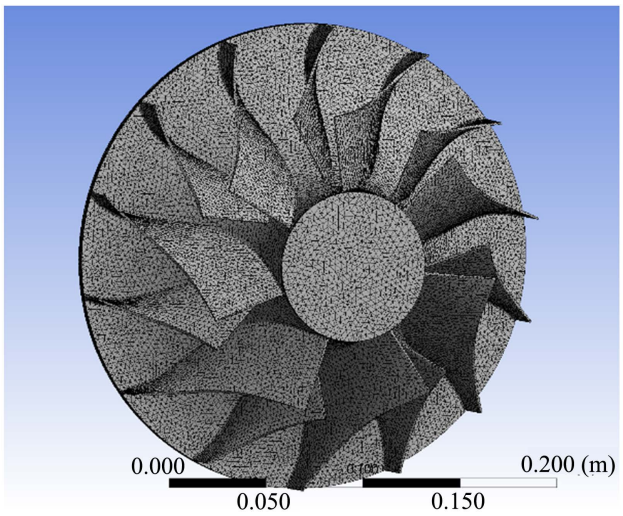

Figure 16. Grid model of impeller.

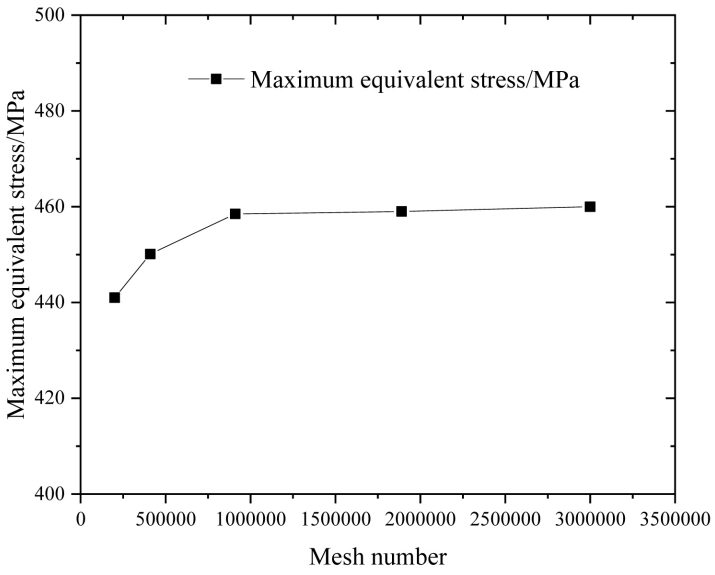

Figure 17. Mesh independency investigation.

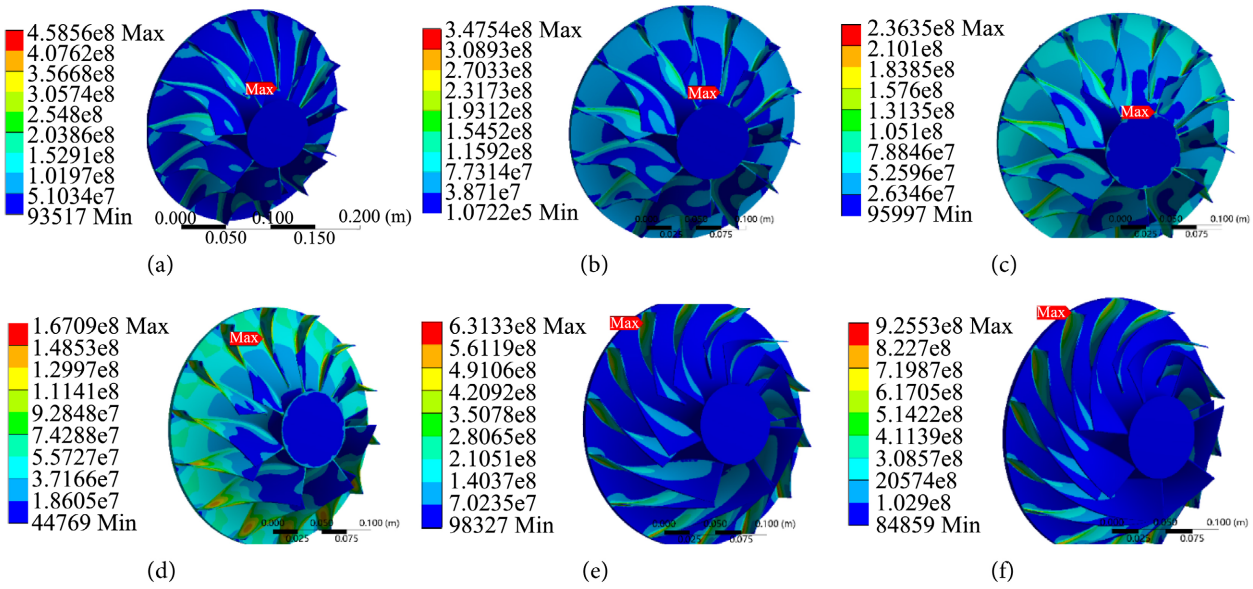

Figure 18. Equivalent stress contours. (a) $\beta_{2B} = 0^{\circ}$; (b) $\beta_{2B} = 10^{\circ}$; (c) $\beta_{2B} = 20^{\circ}$; (d) $\beta_{2B} = 30^{\circ}$; (e) $\beta_{2B} = 40^{\circ}$; (f) $\beta_{2B} = 50^{\circ}$.

Table 3. Material parameters.

Material	Density/(Kg/m^3)	Young's modulus/GPa	Shear modulus/GPa	Ultimate strength/MPa	Yield limit/MPa	Poisson's ratio
aluminium alloy	2730	70	26.5	310	276	0.3

Table 4. Maximum equivalent stress of impellers.

NO.	β_{2B}/°	Maximum equivalent stress
1	0	458 MPa
2	10	347 MPa
3	20	236 MPa
4	30	167 MPa
5	40	631 MPa
6	50	925 MPa

In the range of 0° - 30° of the blade outlet backsweep angle β_{2B}, the maximum equivalent stress of the impeller decreases with the increase of angle, and in the range of 40° - 60°, the maximum equivalent stress of the impeller increases with the increase of blade outlet backsweep angle. This is mainly because the blade of the impeller is a non-radial structure, the centrifugal stress of the blade increases with the increase of the blade outlet backsweep angle. When the blade outlet backsweep angle is equal to 30°, the equivalent stress distribution of the impeller is more uniform, the maximum equivalent stress is the smallest.

10. Conclusions

Six impellers with blade outlet backsweep angle β_{2B} equal to 0°, 10°, 20°, 30°, 40°,

and 50˚ were designed to evaluate the influence of impeller backsweep angle β_{2B} on the performance and characteristics of gas flow using computational fluid dynamics (CFD). The following conclusions can be drawn:

1) The total pressure ratio decreases with the increase of mass flow rate. The larger the blade outlet angle is, the smaller the pressure ratio becomes. The performance curve for the blade outlet backsweep angle β_{2B} of 50˚ has the largest stable operating range among others. The stable operating range with the blade outlet backsweep angle β_{2B} equal to 50˚ is about 3 times more than that with the blade outlet backsweep angle β_{2B} equal to 0˚. In order to achieve the same flow rate and pressure ratio as the impeller with a low back angle, it is necessary to increase the impeller speed or increase the impeller outlet radius.

2) The isentropic efficiency decreases with the increase of mass flow rate. In the range of blade outlet backsweep angle of 0˚ - 40˚, the larger the blade outlet backsweep angle is, the larger isentropic efficiency becomes. Both the isentropic efficiency and operating ratio of the impeller with the blade outlet backsweep angle β_{2B} equal to 50˚ are smaller than those with the blade outlet backsweep angle β_{2B} equal to 40˚. The isentropic efficiency of the impeller with backsweep angle β_{2B} equal to 40˚ is 16.8% - 25.9% higher than that of the impeller with backsweep angle β_{2B} equal to 0˚.

3) The power decreases with the increase of blade outlet backsweep angle at the same flow rate. When the backsweep angle β_{2B} is equal to 0˚ and 10˚, the power increases monotonously with the increase of the mass flow rate. However, the power increases first and then decreases with the increase of mass flow rate when the backsweep angle β_{2B} is equal to 20˚, 30˚, 40˚, and 50˚.

4) The numerical results were subjected to the empirical correlation development to assist the design and optimize parameters of the blade to improve the impeller performance. The fitted data are agreeing with the numerical data within ±15%, ±15% and ±15% except for few points, for total pressure ratio (Π_{tot}), isentropic efficiency (η) and power (P), respectively.

5) In the test case of design centrifugal compressors shown on the blade to blade surface, the velocity at the blade leading edge appears to be higher than that at the blade trailing edge. When the blade outlet backsweep angle β_{2B} is equal to 40˚, the secondary flow effect is the weakest among the designs with different blade outlet backsweep angle β_{2B}.

6) With the increase of the blade outlet backsweep angle of the blade outlet, the position of the maximum equivalent stress shifts from the inlet tip to the outlet. When the blade outlet backsweep angle is equal to 50˚, the maximum equivalent stress occurs at the root of the blade outlet. When the blade outlet backsweep angle is equal to 30˚, the equivalent stress distribution of the impeller is more uniform, the maximum equivalent stress is the smallest.

7) In the paper, the numerical results are subjected to the empirical correlation development to assist the design and optimize the parameters of the blade to improve impeller performance. In future work, it is necessary to further study

the influence of blade outlet backsweep angle of 40˚ - 50˚ on impeller performance and the role of other impeller parameters in impeller optimization design.

Funding Statement

Effects of Near-critical Nonequilibrium Phase-change on the Internal Flow and Aerodynamic Performance of Supercritical CO_2 Compressor (National Natural Science Foundation of China (NSFC), No.: 52006216).

Conflicts of Interest

The authors declare that they have no conflicts of interest to report regarding the present study.

References

[1] Brebenel, M. (2020) An Analytical Method for Simulation of Centrifugal Compressors. *Incas Bulletin*, **12**, 35-49. https://doi.org/10.13111/2066-8201.2020.12.1.4

[2] Xue, X., Wang, T., Zhang, T. and Yang, B. (2018) Mechanism of Stall and Surge in a Centrifugal Compressor with a Variable Vaned Diffuser. *Chinese Journal of Aeronautics*, **31**, 1222-1231. https://doi.org/10.1016/j.cja.2018.04.003

[3] Bonaiuti, D., and Zangeneh, M. (2006) On the Coupling of Inverse Design and Optimization Techniques for Turbomachinery Blade Design. ASME Paper No. GT2006-90897, 1431-1444. https://doi.org/10.1115/GT2006-90897

[4] Geng, M.F., Song, Y.T., Cheng, A.Y. and Feng, H.S. (2020) Numerical Simulation of the Influence of Tip Clearance on the Performance of Centrifugal Cold Compressor. *International Journal of Fluid Machinery and Systems*, **13**, 214-221. https://doi.org/10.5293/IJFMS.2020.13.1.214

[5] Senoo, Y. (1987) Pressure Losses and Flow Field Distortion Induced by Tip Clearance of Centrifugal and Axial Compressors. *JSME International Journal*, **30**, 375-385. https://doi.org/10.1299/jsme1987.30.375

[6] Pelz, P.F. and Karstadt, S. (2010) Tip Clearance Losses—A Physical Based Scaling Method. *International Journal of Fluid Machinery and Systems*, **3**, 1301-1303. https://doi.org/10.5293/IJFMS.2010.3.4.279

[7] Benini, E., Biollo, R. and Ponza, R. (2011) Efficiency Enhancement in Transonic Compressor Rotor Blades Using Synthetic Jets: A Numerical Investigation. *Applied Energy*, **88**, 953-962. https://doi.org/10.1016/j.apenergy.2010.08.006

[8] Shibata, T., Yagi, M., Nishida, H., Kobayashi, H. and Tanaka, M. (2011) Performance Improvement of a Centrifugal Compressor Stage by Increasing Degree of Reaction and Optimizing Blade Loading of a 3D Impeller. *Journal of Turbomachinery*, **133**, 1-8. https://doi.org/10.1115/1.4000565

[9] Khan, A., *et al.* (2020) Blade Meridional Profile Optimization for Novel High-Pressure Ratio Centrifugal Compressor Design Using Numerical Simulations. 3*rd International Conference on Computing, Mathematics and Engineering Technologies-iCoMET*, Sukkur, 29-30 January 2020, 1-9. https://doi.org/10.1109/iCoMET48670.2020.9073850

[10] Xu, C. and Amano, R.S. (2012) Meridional Considerations of the Centrifugal Compressor Development. *International Journal of Rotating Machinery*, **2012**, Article ID: 518381. https://doi.org/10.1155/2012/518381

[11] Rathore, A.S. and Ravichandrakumar, K.B. (2017) Parametric Study on Impeller Exit Blade Width Variation on Centrifugal Compressor. *International Journal of Aerospace and Mechanical Engineering*, **4**, 16-22.

[12] Xie, H., Song, M., Liu, X., Yang, B. and Gu, C. (2018) Research on the Simplified Design of a Centrifugal Compressor Impeller Based on Meridional Plane Modification. *Applied Sciences*, **8**, Article 1339. https://doi.org/10.3390/app8081339

[13] Mojaddam, M. and Pullen, K.R. (2019) Optimization of a Centrifugal Compressor Using the Design of Experiment Technique. *Applied Sciences*, **9**, Article 9020291. https://doi.org/10.3390/app9020291

[14] Ju, Y.P. and Zhang, C.H. (2014) Design Optimization and Experimental Study of Tandem Impeller for Centrifugal Compressor. *Journal of Propulsion and Power*, **30**, 1490-1501. https://doi.org/10.2514/1.B34933

[15] Torshizi, S.A.M., Benisi, A.H. and Durali, M. (2016) Numerical Optimization and Manufacturing of the Impeller of a Centrifugal Compressor by Variation of Splitter Blades. *In Proceedings of the ASME Turbo Expo* 2016: *Turbomachinery Technical Conference and Exposition*, Seoul, 13-17 June 2016.

[16] Wang, X., Xi, G. and Wang, Z. (2006) Aerodynamic Optimization Design of Centrifugal Compressor's Impeller with Kriging Model. *Proceedings of the Institution of Mechanical Engineers*, *Part A Journal of Power Energy*, **220**, 589-597. https://doi.org/10.1243/09576509JPE201

[17] Gu, H.D., Zhou, X.Y., Chen, Y.P., Wu, J.F., Wu, Z., Jiang, Y.H. and Sunden, B. (2021) Analysis, Modeling and Simulations of an Innovative Sliding Vane Rotary Compressor with a Rotating Cylinder. *Energy Conversion and Management*, **230**, 1-13. https://doi.org/10.1016/j.enconman.2020.113822

[18] Yu, Y.Z. (2005) Volumetric Compressor Technical Manual. China Machine Press, Beijing, 693-715.

[19] Rehman, M.M.U., Cheema, T.A., Ahmad, F., Khan, M. and Abbas, A. (1981) Thermodynamic Assessment of Microchannel Heat Sinks with Novel Sidewall Ribs. *Journal of Thermophysics and Heat Transfer*, **34**, 1-12.

Nomenclature

R_{1H}	Impeller inlet hub radius (mm)
R_2	Impeller outlet radius (mm)
n	Impeller rotating speed (r/min)
Π_{tot}	Total pressure ratio
P	Power (kW)
Q_m	Mass flow rate (kg/s)
$p_{tot,i}$	Time-averaged total pressure at the entrance section (Pa)
$h_{isen}/h_{in}/h_{out}$	Specific enthalpy (kJ/kg)
ρ_f	Density of the working fluid (kg/m^3)
k_f	Thermal conductivity (W·m^{-2}·K^{-1})
$a/b/c$	Fitted coefficient
$C_{\theta 2}/C_{\theta 2\infty}$	Tangential velocity component of the blade exit
β_2	Relative airflow angle of the blade exit
β_{1B}	Inlet blade angle (deg)
B_2	Impeller outlet width (mm)
β_{2B}	Blade outlet backsweep (deg)
π	Circumference ratio
η	Isentropic efficiency (%)
y_+	Normalized wall distance
$p_{tot,o}$	Time-averaged total pressure at the outlet (Pa)
μ_f	Dynamic viscosity (Pa·s)
T_f	Temperature of the working fluid (K)
C_{pf}	Constant specific heat capacity (J·kg^{-1}·K^{-1})
U_2	Circle line speed of the blade exit
C_{m2}	Meridian velocity of the blade exit